

# Unveiling Nickel Chemistry in Stabilizing High-Voltage Cobalt-rich Cathodes for Lithium-Ion Batteries

*Moonsu Yoon, Yanhao Dong, Youngbin Yoo, Seungjun Myeong, Jaeseong Hwang, Junhyeok Kim, Seong-Hyeon Choi, Jaekyung Sung, Seok Ju Kang, Ju Li\* and Jaephil Cho\**

M. Yoon, Y. Yoo, S. Myeong<sup>[+]</sup>, J. Hwang, J. Kim, S. -H. Choi, J. Sung, Prof. S. J. Kang, Prof. J. Cho  
Department of Energy Engineering, School of Energy and Chemical Engineering, Ulsan National  
Institute of Science and Technology (UNIST), 50 UNIST-gil, Ulsan 44919, Republic of Korea  
E-mail: jpcho@unist.ac.kr

Y. Dong, Prof. J. Li  
Department of Nuclear Science and Engineering & Department of Materials Science and Engineering,  
Massachusetts Institute of Technology, Cambridge, Massachusetts 02139, United States  
E-mail: liju@mit.edu

[+]Present address : Department of Materials, University of Oxford, Parks Road, Oxford OX1 3PH, UK

**Keywords :** Lithium-ion batteries, cathode degradation, Co-rich cathode, surface reactivity management, cathode-electrolyte interphase

**Abstract:** We present a practical solution to increase the stability of 4.45 V LiCoO<sub>2</sub> via high-temperature Ni doping, without adding any extra synthesis step or cost. We identify how a putative uniform bulk doping with highly soluble elements can profoundly modify the surface chemistry and structural stability from systematic chemistry and microstructure analysis. This modification has an electronic origin, where surface-oxygen-loss induced Co reduction that favors tetrahedral site and causes damaging spinel phase formation is replaced by Ni reduction that favors octahedral site and creates a better cation-mixed structure. Our findings point to many unknown surface effects on the electrochemical performance of battery electrode materials hidden behind extensively practiced bulk doping strategy. The new understanding of complex surface chemistry is expected to help develop higher-energy-density cathode materials for battery applications.

## 1. Introduction

Lithium-ion batteries (LIBs) underly the energy infrastructure of our society. <sup>[1-4]</sup> Significant improvement in volumetric energy density is still in great demand today. For LIB cathodes, even though much progress has been made in Ni-rich layered cathode including the family of LiNi<sub>1-x-y</sub>Co<sub>x</sub>Mn<sub>y</sub>O<sub>2</sub> (NCM) and LiNi<sub>1-x-y</sub>Co<sub>x</sub>Al<sub>y</sub>O<sub>2</sub> (NCA) chemistries (including single crystal

NCM/NCA with  $\sim 3.6 \text{ g cc}^{-1}$  electrode density), conventional  $\text{LiCoO}_2$  (LCO) still holds the record for practical volumetric energy density ( $2600 \text{ Wh L}^{-1}$  when charged to  $4.40 \text{ V vs. Li/Li}^+$ ; higher charge voltage is required to compete with single crystal NCM/NCA) due to its high compressed electrode density ( $4.0\text{--}4.2 \text{ g cc}^{-1}$ ).<sup>[5-7]</sup> As a result, in applications where volume is the most precious and price is less of a problem (e.g. in smartphones), LCO would still hold a large portion of the market in the near future. Elevating the upper cut-off voltage in charging is the most straightforward method to further increase the energy density of LCO, but it unfortunately leads to poor cyclability if charged to  $>4.40 \text{ V vs. Li/Li}^+$  ( $x \geq 0.6$  in the form of  $\text{Li}_{1-x}\text{CoO}_2$ ).<sup>[8-13]</sup> Extensive researches in the past decades seek to address this critical issue. It is known that oxygen redox ( $\text{O}^{2-} \leftrightarrow \text{O}^{1-}$ ) starts to contribute capacity at these higher voltages, since the O  $2p$  orbitals hybridizes with the Co  $3d$  orbitals in the  $\text{Co}^{3+/4+} : t_{2g}$  & O  $2p$  resonant band at lower electronic energies.<sup>[14]</sup> The peroxide ion  $\text{O}^{1-}$  has higher ionic mobility than the oxide ion  $\text{O}^{2-}$ , and  $\text{O}^{1-}$  near the surface are especially prone to leaving the LCO particle, which can happen even when there is no external current (i.e. the battery is supposed to be holding its charge). This disrupts the cathode-electrolyte interphases (CEIs), and the effluent oxygen will react with liquid electrolyte and burn up this scarce resource (only few gram(electrolyte)/Ah used in practical full-cells), leaving voids and reduced transition metals (TM) behind. What then happen afterwards inside LCO are not very clear, but there are theories and practices about mitigating the ill effects, by either (i) suppressing irreversible phase transformations in the bulk LCO by bulk doping (e.g. Mg, Cr, Ti, Mn, and Al; Al/La co-doping)<sup>[15-21]</sup> or (ii) suppressing surface instabilities, by engineering LCO surface via various coating process (e.g. sol-gel process, chemical polymerization or deposition techniques).<sup>[22-26]</sup> While in practice both approaches improve the performance of LCO, the “bulk-phase” versus “surface-phase” dichotomy of this discussion seems a bit self-contradictory, since if mechanism (i) dominates, method (ii) should not work; and *vice versa*, if mechanism (ii) dominates, method (i) should not work. This is the scientific question we seek to address: what is the degradation mechanism of LCO and why both bulk doping and surface coating strategies help? Henceforth, through a sequence of carefully controlled experiments, we found how a putative uniform

bulk doping could significantly affect the surface chemistry by surface segregation of Ni, and to show the “surface-phase” instability theory is correct. Surface segregation by bulk doping small amount of Ni is sufficient to reduce the degree of O anion redox near the surface, because the higher fraction of Ni on surface contributes to capacity without coupling to O  $2p$  orbitals, due to the higher electronic energies of  $\text{Ni}^{3+/4+}:e_g$  compared to  $\text{Co}^{3+/4+}:t_{2g}$  & O  $2p$  resonant band. The surface-enriched Ni also guides the O-loss induced instability toward a more stable surface cation-mixed-phase outcome, rather than an unstable surface spinel-phase outcome that exacerbates the O-loss in a chain-reaction fashion.

In terms of practical applications, since LCO has already enjoyed great success in commercialization, we emphasize that any acclaimed improvements should be verified under industry-level conditions and the method should be cost-effective. These requirements shall be strictly followed in the present study. In this article, we show bulk-phase  $\text{LiCo}_{0.95}\text{Ni}_{0.05}\text{O}_2$  (LCNO) has superior stability at high charge voltage of 4.45 V at practical conditions (loading density  $\sim 15 \text{ mg cm}^{-2}$ , electrode density  $\sim 4.0 \text{ g cm}^{-3}$  and areal capacity  $2.5 \text{ mAh/cm}^2$  with both coin-type half-cell and pouch-type full-cell testing). Previously, the effect of bulk Ni doping (and other elements such as Mg, Zr, and La) was interpreted as a “pillar effect”:  $\text{Ni}^{2+}$  sharing similar charge and ionic radius as  $\text{Li}^+$  would substitute at Octa-3a site in the Li-slab, thus preventing slab sliding at highly delithiated state.<sup>[27, 28]</sup> While we do witness improved cyclability and suppressed bulk phase transitions upon bulk Ni doping, the previous interpretation should not be taken without challenge. While Ni doping only slightly changes the bulk chemistry, more pronounced surface effects, such as suppressed CEI formation and phase transformation in the close-to-surface region, were totally overlooked in the past.

## 2. Results and Discussion

Single crystalline LCNO ( $D_{50}$  of  $\sim 10 \mu\text{m}$ ) with the composition of “ $\text{LiCo}_{0.95}\text{Ni}_{0.05}\text{O}_2$ ” and undoped LCO were prepared by conventional solid-state synthesis (see their microstructures in Figure S1, particle sizes and specific surface areas in Table S1, and chemical compositions and distributions were confirmed by transmission electron microscopy coupled with an energy dispersive X-ray

spectrometer in Figure S2 and inductively coupled plasma-optical emission spectrometry in Table S2, respectively, Supporting Information). To obtain crystallographic parameters and atomic occupancies, Rietveld refinement was performed, which shows 0.9% Ni out of the total number of TM is located at Li-layer sites (LiL) in LCNO (Figure S3 and detailed fitting parameters in Table S3, Supporting Information). This anti-site defect Ni<sub>LiL</sub> (so-called “cation mixing”) forms because of similar charge and ionic radius of Ni<sup>2+</sup> and Li<sup>+</sup>, whose mixing level becomes larger at higher temperatures and in a less-oxidizing atmosphere where Ni<sup>2+</sup> is thermodynamically favored over Ni<sup>3+</sup>.<sup>[29, 30]</sup> Apparently, this high level of cation mixing in LCNO (relative to the amount of Ni we put in) comes from the synthesis condition (i.e. high temperature of 970 °C in air).

The electrochemical properties of LCNO were first evaluated by half-cells at 3.0–4.45 V vs. Li/Li<sup>+</sup>, and the cyclic performance at a current rate of 1.0 C (185 mA g<sup>-1</sup>) are displayed in Figure 1a and b (the formation cycle for each cell was conducted at 0.1 C, Figure S4, Supporting Information). Interestingly, LCNO have demonstrated the better cycling stability with a high capacity retention of ~93% (165 mAh g<sup>-1</sup>) during 100 cycles, compared to ~73% capacity retention (131mAh g<sup>-1</sup>) of LCO. LCNO also has a higher average Coulombic efficiency (CE) of 99.69% for the first 100 cycles, compared to that of 98.72% for LCO, when charged to 4.45 V vs. Li/Li<sup>+</sup>. Furthermore, the charge/discharge curves of LNCO have rarely changed, while that of LCO exhibits a dramatic change upon cycling (Figure 1b). Meanwhile, as shown in Figure 1c, LCNO also demonstrates better rate performance than LCO, with less capacity decrease from 0.2C (0.51 mA cm<sup>-2</sup>) to 5C (12.80 mA cm<sup>-2</sup>). Specifically, LCNO demonstrated an impressive discharge capacity of 150.2 mAh g<sup>-1</sup> at 5 C with less overpotentials, while LCO has only 116.2 mAh g<sup>-1</sup> at 5 C (Figure S5, Supporting Information).

Next, to evaluate the long-term cycling performance of LCNO in a more practical way, pouch-type full-cell testing was performed in the *full-cell* voltage range of 3.0–4.35 V (Figure 1d). Spherical graphite (Gr) is used as anode in full-cells, exhibiting stable cycling properties with an average voltage of 0.15 V in the Gr/Li half-cell (Figure S6, more details on electrode specifications, testing

conditions and energy density calculation method are given in Table S4 and Note S1, Supporting Information). LCNO/Gr full-cell shows better cycling stability and higher CE than LCO/Gr at both 25 °C (Figure 1d and S7) and 45 °C (Figure S8, Supporting Information), which agree with the half-cell results. Specifically, at 25 °C, LCNO/Gr full-cell demonstrates superior energy density of 601 Wh L<sup>-1</sup> (92% retention) after 500 cycles, compared with 514 Wh L<sup>-1</sup> (79% retention) for LCO/Gr. Moreover, the working voltage (average discharge voltage) of LCNO/Gr full-cell stably maintains at around 3.82V over 500 cycles, while that of LCO/Gr gradually drops to 3.78V. Therefore, LCNO demonstrates superior electrochemical performance in both half- and full-cell over LCO at the high voltage.

Now that the experimental advantage of slight Ni bulk doping is obvious, we seek to understand the underlying mechanism. As mentioned above, previous studies attributed (A) improved cyclability of Ni doped LCO to a “pillar effect” based on the observation of concurrent (B) suppressed phase transitions at high voltages (i.e. the case showing both A and B). The latter was also observed in the present work, as illustrated in the differential capacity vs. voltage ( $dQ/dV$ ) plot of the first charge/discharge curve of in Figure 2a. There are two peaks at 4.1 V and 4.2 V due to the phase transition from the hexagonal (O3) to monoclinic phase<sup>[31]</sup> and the other peak at 4.4V represents the O3–(H1-3) phase transition in LCO<sup>[32, 33]</sup>, while they become much weaker in LCNO. However, to explain (A) improved cyclability by (B) suppressed phase transitions in the bulk needs more thoughtful considerations. First of all, the transformed phases such as O2-type LCO have high electrochemical capacity as well as high Li<sup>+</sup> and electronic conductivities, so it is not straightforward why such bulk phase transitions necessarily lead to degradation.<sup>[34]</sup> Second, surface coating has been frequently practiced to improve high-voltage cyclability of LCO. While its benefit is undeniable, it does not suppress any bulk phase transitions at all (i.e. the case showing A but not B).<sup>[24, 35, 36]</sup> Third, some studies of bulk doping show suppressed phase transitions yet there were no improvements in high-voltage cyclability (i.e. the case showing B but not A).<sup>[37]</sup> So (B) is neither a necessary nor sufficient condition of (A). Furthermore, according to ex-situ X-ray diffraction (XRD) of cycled LCO

and LCNO in Figure 2b and Figure S9 (Supporting Information), the irreversible bulk phase transition in LCO (from O3 to H1-3, evidenced by shifting of (003) peak at  $2\theta=18.9^\circ$  and fading of (006) peak at  $38.4^\circ$ ) does not occur during the first 100 cycles, yet the capacity decay is continuous from the very beginning and accelerated degradation starts from early 20 cycles. Therefore, although Ni doping does suppress bulk phase transitions during charge-discharge process, it cannot be the main reason for the improved cyclability. Meanwhile, we noted marginal effect of 5% Ni on the bulk redox of LCO. The  $dQ/dV$  curve of LCNO has similar shape with LCO (Figure 2a), except for the early stage of charge below 3.9 V due to  $\text{Ni}^{3+/4}$  redox. [38] This conclusion is further supported by first-principles calculations, which identify similar electronic density of states (DOS) for LCO (Figure S10 for stoichiometric  $\text{LiCoO}_2$  and to be shown in Figure 5b for delithiated  $\text{Li}_{0.333}\text{CoO}_2$ , Supporting Information) and LCNO (Figure S11 for stoichiometric  $\text{LiNi}_{0.074}\text{Co}_{0.926}\text{O}_2$  and Figure S12 for delithiated  $\text{Li}_{0.333}\text{Ni}_{0.074}\text{Co}_{0.926}\text{O}_2$ , Supporting Information). These observations leave an intriguing question: If suppressing bulk phase transitions does not help much and bulk redox thermochemistry is barely changed, how could bulk Ni doping work?

Before answering the question, we first investigate whether the degradation has a thermodynamic or kinetic origin, via galvanostatic intermittent titration technique (GITT) characterizations for LCO and LCNO conducted at 1<sup>st</sup>, 50<sup>th</sup> and 100<sup>th</sup> cycles (Figure 2c and d). For pristine LCO and LCNO, the overpotentials are small at all states of charge (except for the end of discharge), indicating good transport kinetics of  $\text{Li}^+$  and electrons in the electrode composites (of active materials, carbon, binder and electrolyte-soaked porosity). Yet, for LCO, 4.45V-cycling induced a dramatic overpotential growth, while the increment is much smaller in LCNO. Interestingly, if we exclude such voltage losses (i.e. overpotential) due to either  $\text{Li}^+$  or electron transport (in either electrode composites or LCO/LCNO particles) and plot the relaxed potentials after each titration step as a function of discharge capacity (mimicking charge/discharge curve under open circuit condition), the data before and after cycling coincide into one curve nicely for both LCO and LCNO (Figure 2e and f; more detailed provided in Note S2, Supporting Information). It clearly demonstrates that

capacity decay in LCO and LCNO is mostly from growth of internal impedance from sluggish kinetics rather than changes in redox chemistry and thermodynamics.<sup>[24, 39]</sup> The conclusion is further supported by electrochemical impedance spectroscopy (EIS) measurements, which show over-growth of charge transfer resistance (calculated from the semicircle radius of the middle-to-low frequencies) in the Nyquist plots of cycled LCO, while the change is much smaller in LCNO (Figure S13, Supporting Information). We also noted that the XRD results indicate minimum structural change of both LCO and LCNO during the first 100 cycles (Figure S9, Supporting Information), thus the accelerated capacity decay in LCO cells cannot be dominantly influenced by irreversible structural changes in the bulk materials either. Without any evident changes in either redox chemistry or atomic structure and with clearly observed impedance growth, we conclude that the degradation of doped/undoped LCO is critically coupled with a kinetic rather than a thermodynamic origin.

We now provide a simple, consistent explanation of the above seemingly disparate observations: A putative uniform Ni doping also modifies the surface of LCO by surface segregation, which is critical to its electrochemical stability. This is supported by the following experimental findings. First, the surface of pristine LCO particles has a layered structure (space group  $R\bar{3}m$ , same with bulk phase) as shown by TEM in Figure S14 (Supporting Information). However, it reconstructs extensively after cycling, in the form of phase transition to  $Co_3O_4$ -like spinel structure (space group  $Fd\bar{3}m$ , 5-10 nm thick after 100 cycles; it is known to have sluggish  $Li^+$  diffusivity)<sup>[40]</sup> and microcrack formation as shown in **Figure 3a** and **b**. Furthermore, the high-angle annular dark-field (HAADF) signal intensity significantly decreased at the surface, indicating a large amount of TM defects were generated after cycling (Figure 3c), or a rough surface. In contrast, the surface of LCNO has a cation-mixed layered structure with ~3 nm thickness before (Figure S15, Supporting Information) and after cycling (Figure 3d and e) and no microcracks were observed. Little variations of HAADF signal (Figure 3f) from the surface to the bulk indicates much less TM defects/surface roughness compared to LCO. (Ni segregation at the surface of LCNO is supported by spatially-resolved electron energy-loss spectroscopy (EELS) data of pristine and cycled LCNO in Figure Sx.) Therefore, Ni doping modifies

the surface structure of LCO, which does not evolve as significant as undoped LCO upon cycling.

Second, spatially-resolved EELS reveals less reduction of Co at the surface of LCNO than LCO after 1<sup>st</sup> charge and after 100<sup>th</sup> discharge (Figure 3g-i). ( $L_3/L_2$  intensity ratios of standard references  $\text{LiCoO}_2$ ,  $\text{Co}_3\text{O}_4$ , and  $\text{CoO}$  were used to identify  $\text{Co}^{3+}$ ,  $\text{Co}^{2.666+}$ , and  $\text{Co}^{2+}$ , respectively; for more details, see Figure S16, S17 and Note S3, Supporting Information). In pristine LCO, we found constant valence/local chemical environment of  $\text{Co}^{3+}$  at 0-35 nm from the surface (Figure 3h). However, when LCO is firstly charge to 4.45 V vs.  $\text{Li}/\text{Li}^+$ , Co at the surface becomes lower in valence, which is in contrast with oxidation of Co in the bulk (to compensate charge of delithiation). The surface reduction implies massive side reaction between charged LCO and electrolytes, leading to significant surface reconstruction.<sup>[41-43]</sup> This process continues upon cycling, resulting in greatly reduced Co close to  $\text{Co}^{2.666+}$  after 100 cycles, which is consistent with the observed  $\text{Co}_3\text{O}_4$ -like structure in Figure 3b. In contrast, Co is less reduced in LCNO than in LCO, implying that less side reactions and surface reconstruction (right panel of Figure 3h). One thing to note is that even though some  $\text{Ni}^{3+}$  are reduced to +2 at the surface of LCNO (decrease in shoulder peak of  $\text{Ni}^{3+}$  species, at  $\sim 854$  eV, in Figure 3i)<sup>[44]</sup>, its surface remains similarly cation-mixed structure before and after cycling.

Considering the strong correlations (but with time delays) between oxygen anion-redox, oxygen mobility and loss, surface instability and cation transformations at high voltage, the investigation of surface oxygen states would shed light on the mechanism of improvement by Ni doping. In O K-edge, the pre-edge corresponds to transition from O core  $1s$  to the unoccupied hybridized band state of O  $2p$  and TM  $3d$  orbitals, indicating the hole states in TM–O bonding.<sup>[45]</sup> Interestingly, when the prepared cathodes were firstly charged to 4.45V, we observed a small shoulder (at 528-533 eV) for LCO outer surface but not for LCNO (Figure 3j and Figure S18, Supporting Information), which indicates an suppressed oxidation of  $\text{O}^{2-}$  in LCNO surface during charge.<sup>[13, 46]</sup> Since the oxidation of  $\text{O}^{2-}$  (forming mobile peroxy  $\text{O}^{1-}$ ) results in serious side reactions due to oxygen loss and high chemical reactivity toward electrolyte, we believe less  $\text{O}^{1-}$  generation *on surface* must be beneficial.<sup>[47-49]</sup> Ni segregation helps in this regard, because the higher fraction of Ni on surface

contributes to capacity without coupling to O  $2p$  orbitals, due to the higher electronic energies of Ni<sup>3+/4+</sup>: $e_g$  compared to Co<sup>3+/4+</sup>: $t_{2g}$  & O  $2p$  resonant band.<sup>[14]</sup> Consistently, there is less gas evolution for LCNO than LCO during first charge, as supported by *in situ* differential electrochemical mass spectrometry (DEMS) data in Figure 3k. Therefore, Ni-modified surface structure effectively suppresses oxidation of O<sup>2-</sup> species, thereby experiences less TM reduction and oxygen loss upon charge and cycling.

Third, we conducted floating test (an established method to evaluate the voltage window of electrolytes)<sup>[50, 51]</sup> to investigate the surface reactivity of LCO and LCNO. Half cells after 1<sup>st</sup>, 50<sup>th</sup> and 100<sup>th</sup> cycles (at 0.2C) were charged to 4.45 V vs. Li/Li<sup>+</sup>, maintained under constant voltage for 27 hours under 60 °C while recording the leakage current. During the long-time high-temperature holding, the leakage current must come from side reactions between charged LCO/LCNO and organic electrolyte. As shown in **Figure 4a** and b, the leakage current density of LCO is larger than that of LCNO at initial cycle and their difference magnifies upon cycling. Consistent results were also obtained by performing the same floating tests at higher charge voltage of 4.5–4.7 V vs. Li/Li<sup>+</sup> (Figure S19, Supporting Information), where LCNO always has much smaller leakage current density. Considering the similar particle size and specific surface area (see Brunauer–Emmett–Teller, BET data in Table S1 of LCO and LCNO, Supporting Information), the above results prove Ni-modified surface structure indeed reduces chemical reactivity of LCO toward the organic electrolyte. Since practical full-cells use very little electrolyte (few gram/Ah), this bodes well for the long-term shelf life and cycle life of the LCNO battery.

Fourth, the lowered chemical reactivity results in less CEI formation of LCNO than LCO. This is evidenced by X-ray photoelectron spectroscopy (XPS) and time-of-flight secondary ion mass spectrometry (TOF-SIMS) data collected on LCO and LCNO before and after 100 cycles in half-cell testing. As shown by XPS in Figure 4e, the signal of lattice O<sup>2-</sup> has a strong peak at ~530 eV in pristine LCO and LCNO. However, it decays to zero with an emerging peak at 532-533 eV (from O  $1s$  orbital of oxidation products of electrolytes) for cycled LCO, while its intensity is better

maintained in cycled LCNO. Similarly, there is weaker intensity for the peak at ~56 eV (from Li 1s orbital of Li-containing compound, such as resistive LiF and Li<sub>2</sub>CO<sub>3</sub>) in cycled LCNO than in cycled LCO. In particular, one thing to note is that in C 1s region of cycled LCO, a dramatic increase of the C 1s peak characteristics of C–O (C 1s, 286 eV) and C=O (C 1s, 289 eV) bonds in approximately 2:1 ratio upon cycling would be expected for mass generation of PEC, a result of ethylene carbonate (EC) decomposition (Figure 4f).<sup>[52]</sup> These features coherently suggest that on LCNO surface, side reactions including not only EC ring-opening but also PF<sub>6</sub><sup>−</sup>, counterion of salt, to form PF<sub>5</sub> and HF<sup>[53, 54]</sup>, are significantly suppressed. As illustrated in Figure 4g, consistent trend is also found in TOF-SIMS mapping, showing less accumulation of CEIs species (e.g. <sup>7</sup>LiF<sub>2</sub><sup>−</sup>, C<sub>3</sub>OF<sup>−</sup>, CoF<sub>3</sub><sup>−</sup>, CH<sub>3</sub>O<sup>−</sup>, C<sub>2</sub>HO<sup>−</sup> and C<sub>2</sub>F<sup>−</sup> from electrolyte decomposition)<sup>[55, 56]</sup> on the surface of LCNO than that of LCO (for more details, see Figure S20, S21 and Table S5, Supporting Information). Furthermore, as the floating test at high temperature and high voltage can be viewed as an accelerated degradation experiment, the overgrown CEI enriched with C and F signals on the surface of LCO after 1<sup>st</sup> charge to 4.45 V (vs. Li/Li<sup>+</sup>) and 27 h's hold at 60 °C can be vividly seen under scanning electron microscope (SEM) in Figure 4c and Figure S22 (Supporting Information), while that of LCNO can hardly be detected visually in Figure 4d. Therefore, Ni-modified surface structure indeed reduces the formation and growth of CEI at high voltages and during prolonged cycling.

Lastly, we rationalized the improved surface stability of LCNO via first-principles calculations, by comparing the calculated electronic density of states (DOS) of Li<sub>0.333</sub>CoO<sub>2</sub> in **Figure 5a** (corresponding to delithiated LCO) and Li<sub>0.111</sub>Ni<sub>0.296</sub>Co<sub>0.926</sub>O<sub>2</sub> in Figure 5d (delithiated cation-mixed structure similar to the surface of LCNO, which has the same state of charge as Li<sub>0.33</sub>CoO<sub>2</sub>; here, 0.222 mole Ni per formula is at Li-slab and the remaining 0.074 is at TM-slab, so it can be written as (Li<sub>0.111</sub>Ni<sub>0.222</sub>)(Ni<sub>0.074</sub>Co<sub>0.926</sub>)O<sub>2</sub>. Unlike Li<sub>0.333</sub>CoO<sub>2</sub> which has overlapping valence-band and conduction-band states similar to a semi-metal, Li<sub>0.111</sub>Ni<sub>0.296</sub>Co<sub>0.926</sub>O<sub>2</sub> has a small band gap of 0.3 eV, which reduces DOS at the Fermi level (Figure 5b and 5e). From electronic perspective, this feature lowers the energy of highest occupied states and limits electron transfer from carbonate-based

electrolyte dissociation, thus consequently stabilizing the cathode-electrolyte interface.<sup>[43, 47, 57]</sup> A quantitative comparison between  $\text{Li}_{0.333}\text{CoO}_2$  and  $\text{Li}_{0.111}\text{Ni}_{0.296}\text{Co}_{0.926}\text{O}_2$  is shown in Figure 5c and f, where the total DOS (in black) and projected DOS of O 2p orbitals (in red) at  $-0.8$  to  $0$  eV vs. Fermi level are plotted. Obviously,  $\text{Li}_{0.111}\text{Ni}_{0.296}\text{Co}_{0.926}\text{O}_2$  (Figure 5c) has much less DOS than  $\text{Li}_{0.333}\text{CoO}_2$  (Figure 5f), which supports the experimental findings of its reduced surface reactivity.

With the above information, a unified picture governing the stability and degradation kinetics of LCO/LCNO can be provided, which is schematically plotted in **Figure 6**. For undoped LCO, it suffers from severe surface oxygen loss and Co reduction from +3 to +2 during 1<sup>st</sup> charge. It triggers surface phase transition and cation densification to a  $\text{Co}_3\text{O}_4$ -like spinel structure during discharge ( $\text{Co}^{2+}$  migration to tetrahedral site, which stabilizes the electronic structure of  $\text{Co}^{2+}$ :  $e_g^4 t_{2g}^3$ ;  $\text{Co}_3\text{O}_4$  is a well-known normal spinel structure, with tetrahedral  $\text{Co}^{2+}$  and octahedral  $\text{Co}^{3+}$ ), whose compact structure and small interstitial sites impedes  $\text{Li}^+$  intercalation/diffusion. When this transformed surface layer undergoes charging again, it cannot be delithiated yet  $\text{Co}^{2+}$  is still prone to oxidation, which forces  $\text{Co}_3\text{O}_4$  to decompose, Co ion to dissolve (see data of dissolved Co in electrolyte of cycled LCNO/Gr pouch-type full cell at  $45^\circ\text{C}$  in Table Sx), oxygen to lose, much side reactions to happen, and extensive CEI to form in a chain-reaction fashion. The growth of resistive CEI and  $\text{Co}_3\text{O}_4$ -like surface structure increase the internal impedance continuously, which makes the degradation of LCO an accumulative and self-accelerating process. In comparison, the situation is greatly improved for LCNO. Albeit of smaller extent, LCNO also loses some surface oxygen during the 1<sup>st</sup> charge. But it is accompanied by Ni reduction from +3 to +2, rather than Co. This leaves the surface structure a cation-mixed structure ( $\text{Ni}^{2+}$  migration to octahedral site, because  $\text{Ni}^{2+}$  has a large radius similar to  $\text{Li}^+$  and octahedral crystal field stabilizes  $\text{Ni}^{2+}$ :  $t_{2g}^6 e_g^2$ ), which has larger lattice parameter and allows  $\text{Li}^+$  intercalation/diffusion. Furthermore, Ni-modified cation-mixed structure has lower-energy HOMO, which also reduces the side reactions. Both factors cut off the positive-feedback-loop of accelerated degradation, which contributes the experimentally-confirmed cycling stability of LCNO.

### 3. Conclusion

To summarize, we present a practical solution to increase the stability of 4.45 V LiCoO<sub>2</sub> via high-temperature Ni doping, without adding any extra synthesis steps or cost. This simple method can be combined with further surface modifications and such experiments are in progress to develop stable 4.6 V LiCoO<sub>2</sub>. On the scientific side, we identified how a long putative uniform bulk doping with highly soluble elements can profoundly modify the surface structure and chemistry from systematic chemistry and microstructure analysis, which is critical to the electrochemical performance. This modification has an electronic origin, where surface-oxygen-loss induced Co reduction that favors tetrahedral site and causes damaging spinel phase formation is replaced by Ni reduction (a “sacrificial” cation, bearing the same spirit of sacrificial anodes in corrosion) that favors octahedral site and creates a better cation-mixed structure. Our findings point to many unknown surface effects on the electrochemical performance of battery electrode materials hidden behind extensively practiced bulk doping strategy. The new understanding of complex surface chemistry is expected to help develop higher-energy-density cathode materials for battery applications.

### Acknowledgements

M. Y and Y. D contributed equally to this work. This work was supported by the Korea Institute of Energy Technology Evaluation and Planning (KETEP) and the Ministry of Trade, Industry & Energy (MOTIE) of the Republic of Korea (No. 20172410100140). J.L. and Y.D. acknowledge support by Department of Energy, Basic Energy Sciences under award number DE-SC0002633 (Chemomechanics of Far-From-Equilibrium Interfaces).

### Competing interests

The authors declare no competing financial interests.

### References

- [1] D. Larcher, J. M. Tarascon, *Nat. Chem.* **2014**, 7, 19.
- [2] B. Dunn, H. Kamath, J.-M. Tarascon, *Science* **2011**, 334, 928.
- [3] M. M. Thackeray, C. Wolverton, E. D. Isaacs, *Energy Environ. Sci.* **2012**, 5, 7854.
- [4] J. B. Goodenough, Y. Kim, *Chem. Mater.* **2010**, 22, 587.
- [5] A. Manthiram, J. C. Knight, S.-T. Myung, S.-M. Oh, Y.-K. Sun, *Adv. Energy Mater.* **2016**, 6, 1501010.
- [6] J. Kim, H. Ma, H. Cha, H. Lee, J. Sung, M. Seo, P. Oh, M. Park, J. Cho, *Energy Environ. Sci.*

- 2018**, 11, 1449.
- [7] S. Kalluri, M. Yoon, M. Jo, S. Park, S. Myeong, J. Kim, S. X. Dou, Z. Guo, J. Cho, *Adv. Energy Mater.* **2017**, 7, 1601507.
- [8] T. Ohzuku, A. Ueda, *Solid State Ionics* **1994**, 69, 201.
- [9] J. Cho, Y. J. Kim, B. Park, *J. Electrochem. Soc.* **2001**, 148, A1110.
- [10] Z. Chen, J. R. Dahn, *Electrochim. Acta* **2004**, 49, 1079.
- [11] J. Kikkawa, S. Terada, A. Gunji, T. Nagai, K. Kurashima, K. Kimoto, *J. Phys. Chem. C* **2015**, 119, 15823.
- [12] J.-N. Zhang, Q. Li, Y. Wang, J. Zheng, X. Yu, H. Li, *Energy Storage Mater.* **2018**, 14, 1.
- [13] R. Hausbrand, G. Cherkashinin, H. Ehrenberg, M. Gröting, K. Albe, C. Hess, W. Jaegermann, *Mater. Sci. Eng., B* **2015**, 192, 3.
- [14] A. Manthiram, *ACS Central Science* **2017**, 3, 1063.
- [15] H.-J. Kim, Y. U. Jeong, J.-H. Lee, J.-J. Kim, *J. Power Sources* **2006**, 159, 233.
- [16] J. H. Cheng, C. J. Pan, C. Nithya, R. Thirunakaran, S. Gopukumar, C. H. Chen, J. F. Lee, J. M. Chen, A. Sivashanmugam, B. J. Hwang, *J. Power Sources* **2014**, 252, 292.
- [17] S. Madhavi, G. V. Subba Rao, B. V. R. Chowdari, S. F. Y. Li, *Electrochim. Acta* **2002**, 48, 219.
- [18] J. Yu, Z. Han, X. Hu, H. Zhan, Y. Zhou, X. Liu, *J. Power Sources* **2014**, 262, 136.
- [19] A. Liu, J. Li, R. Shunmugasundaram, J. R. Dahn, *J. Electrochem. Soc.* **2017**, 164, A1655.
- [20] F. Zhou, W. Luo, X. Zhao, J. R. Dahn, *J. Electrochem. Soc.* **2009**, 156, A917.
- [21] Q. Liu, X. Su, D. Lei, Y. Qin, J. Wen, F. Guo, Y. A. Wu, Y. Rong, R. Kou, X. Xiao, F. Aguesse, J. Bareño, Y. Ren, W. Lu, Y. Li, *Nat. Energy* **2018**, 3, 936.
- [22] Y.-C. Lu, A. N. Mansour, N. Yabuuchi, Y. Shao-Horn, *Chem. Mater.* **2009**, 21, 4408.
- [23] Y. S. Jung, P. Lu, A. S. Cavanagh, C. Ban, G. H. Kim, S. H. Lee, S. M. George, S. J. Harris, A. C. Dillon, *Adv. Energy Mater.* **2013**, 3, 213.
- [24] J. Qian, L. Liu, J. Yang, S. Li, X. Wang, H. L. Zhuang, Y. Lu, *Nat. Commun.* **2018**, 9, 4918.
- [25] S. Kalluri, M. Yoon, M. Jo, S. Park, S. Myeong, J. Kim, S. X. Dou, Z. Guo, J. Cho, *Adv. Energy Mater.* **2017**, 7, 1601507.
- [26] J. Xie, J. Zhao, Y. Liu, H. Wang, C. Liu, T. Wu, P.-C. Hsu, D. Lin, Y. Jin, Y. Cui, *Nano Res.* **2017**, 10, 3754.
- [27] M. Zou, M. Yoshio, S. Gopukumar, J.-i. Yamaki, *Chem. Mater.* **2005**, 17, 1284.
- [28] W. Cho, S. Myeong, N. Kim, S. Lee, Y. Kim, M. Kim, S. J. Kang, N. Park, P. Oh, J. Cho, *Adv. Mater.* **2017**, 29, 1605578.
- [29] Y. Koyama, H. Arai, I. Tanaka, Y. Uchimoto, Z. Ogumi, *Chem. Mater.* **2012**, 24, 3886.
- [30] H. Chen, J. A. Dawson, J. H. Harding, *J. Mater. Chem. A* **2014**, 2, 7988.
- [31] C. A. Marianetti, G. Kotliar, G. Ceder, *Nature Materials* **2004**, 3, 627.

- [32] A. Van der Ven, M. K. Aydinol, G. Ceder, *J. Electrochem. Soc.* **1998**, 145, 2149.
- [33] Z. Chen, Z. Lu, J. R. Dahn, *J. Electrochem. Soc.* **2002**, 149, A1604.
- [34] J. M. Paulsen, J. R. Mueller-Neuhaus, J. R. Dahn, *J. Electrochem. Soc.* **2000**, 147, 508.
- [35] A. Yano, M. Shikano, A. Ueda, H. Sakaebe, Z. Ogumi, *J. Electrochem. Soc.* **2017**, 164, A6116.
- [36] J.-H. Shim, J.-M. Han, J.-H. Lee, S. Lee, *ACS Appl. Mater. Interfaces* **2016**, 8, 12205.
- [37] Y. Jin, S. Xu, Z. Li, K. Xu, W. Ding, J. Song, H. Wang, J. Zhao, *J. Electrochem. Soc.* **2018**, 165, A2267.
- [38] R. V. Chebiam, A. M. Kannan, F. Prado, A. Manthiram, *Electrochem. Commun.* **2001**, 3, 624.
- [39] H. Gabrisch, R. Yazami, B. Fultz, *J. Electrochem. Soc.* **2004**, 151, A891.
- [40] W. M. Seong, K. Yoon, M. H. Lee, S.-K. Jung, K. Kang, *Nano Lett.* **2018**, 18, 8071.
- [41] G. Cherkashinin, K. Nikolowski, H. Ehrenberg, S. Jacke, L. Dimesso, W. Jaegermann, *Phys. Chem. Chem. Phys.* **2012**, 14, 12321.
- [42] D. Takamatsu, Y. Koyama, Y. Orikasa, S. Mori, T. Nakatsutsumi, T. Hirano, H. Tanida, H. Arai, Y. Uchimoto, Z. Ogumi, *Angew. Chem. Int. Ed.* **2012**, 51, 11597.
- [43] X. Yu, A. Manthiram, *Energy Environ. Sci.* **2018**, 11, 527.
- [44] F. Lin, D. Nordlund, I. M. Markus, T.-C. Weng, H. L. Xin, M. M. Doeff, *Energy Environ. Sci.* **2014**, 7, 3077.
- [45] S. Myeong, W. Cho, W. Jin, J. Hwang, M. Yoon, Y. Yoo, G. Nam, H. Jang, J.-G. Han, N.-S. Choi, *Nat. Commun.* **2018**, 9, 3285.
- [46] W.-S. Yoon, K.-B. Kim, M.-G. Kim, M.-K. Lee, H.-J. Shin, J.-M. Lee, J.-S. Lee, C.-H. Yo, *J. Phys. Chem. B* **2002**, 106, 2526.
- [47] L. Giordano, P. Karayaylali, Y. Yu, Y. Katayama, F. Maglia, S. Lux, Y. Shao-Horn, *J. Phys. Chem. Lett.* **2017**, 8, 3881.
- [48] D. Takamatsu, Y. Koyama, Y. Orikasa, S. Mori, T. Nakatsutsumi, T. Hirano, H. Tanida, H. Arai, Y. Uchimoto, Z. Ogumi, *Angew. Chem. Int. Ed.* **2012**, 51, 11597.
- [49] S. Sharifi-Asl, J. Lu, K. Amine, R. Shahbazian-Yassar, *Adv. Energy Mater.* **2019**, 9, 1900551.
- [50] M. He, L. Hu, Z. Xue, C. C. Su, P. Redfern, L. A. Curtiss, B. Polzin, A. von Cresce, K. Xu, Z. Zhang, *J. Electrochem. Soc.* **2015**, 162, A1725.
- [51] Z. Zhang, L. Hu, H. Wu, W. Weng, M. Koh, P. C. Redfern, L. A. Curtiss, K. Amine, *Energy Environ. Sci.* **2013**, 6, 1806.
- [52] L. Yang, B. Ravdel, B. L. Lucht, *Electrochem. Solid-State Lett.* **2010**, 13, A95.
- [53] J. L. Tebbe, T. F. Fuerst, C. B. Musgrave, *ACS Appl. Mater. Interfaces* **2016**, 8, 26664.
- [54] J. L. Tebbe, T. F. Fuerst, C. B. Musgrave, *J. Power Sources* **2015**, 297, 427.
- [55] W. Li, A. Dolocan, P. Oh, H. Celio, S. Park, J. Cho, A. Manthiram, *Nat. Commun.* **2017**, 8, 14589.

- [56] K. Edström, T. Gustafsson, J. O. Thomas, *Electrochim. Acta* **2004**, 50, 397.
- [57] M. Gauthier, T. J. Carney, A. Grimaud, L. Giordano, N. Pour, H.-H. Chang, D. P. Fenning, S. F. Lux, O. Paschos, C. Bauer, F. Maglia, S. Lupart, P. Lamp, Y. Shao-Horn, *J. Phys. Chem. Lett.* **2015**, 6, 4653.

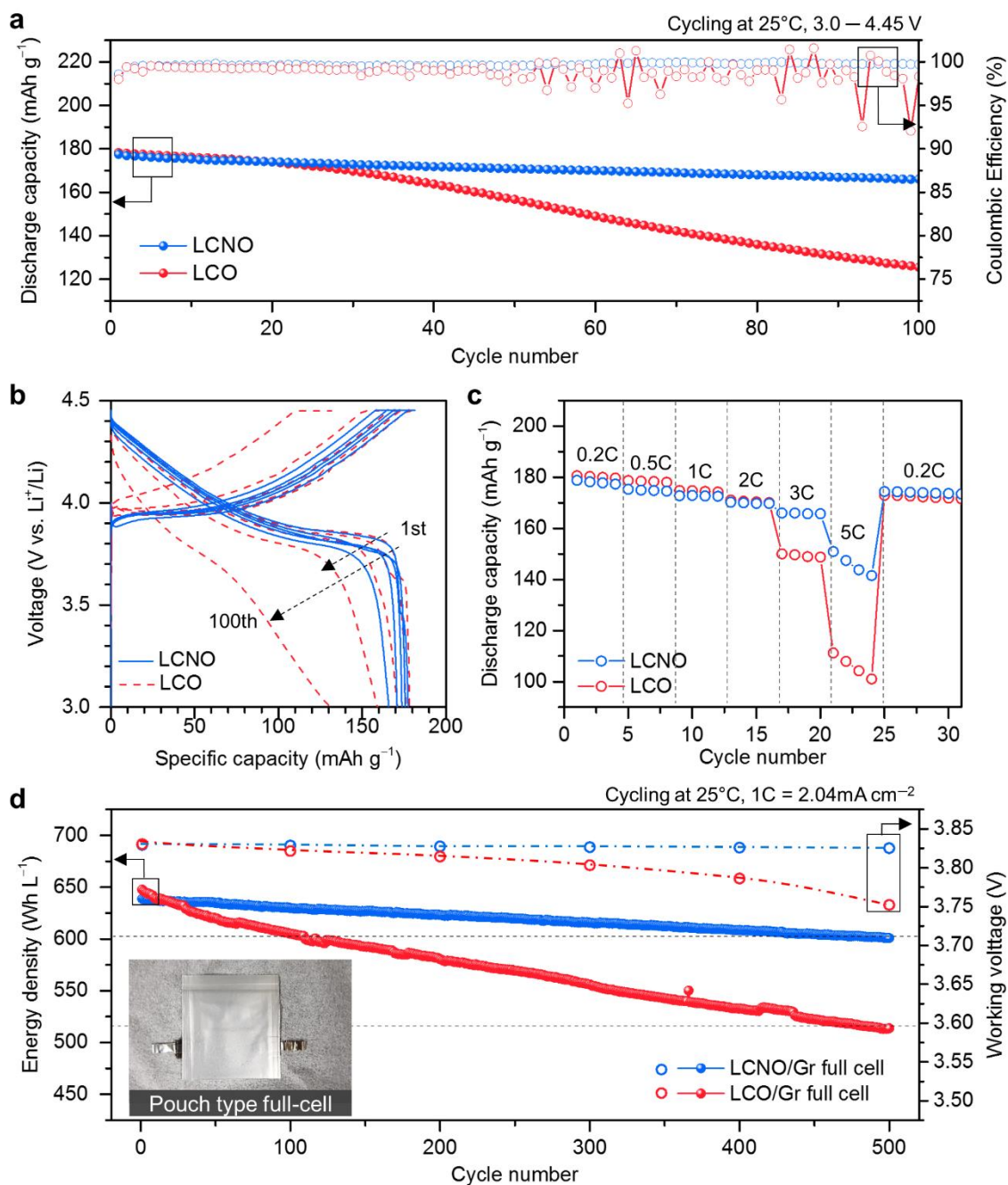


**Figure 1.** Electrochemical performance of LCO and LCNO cells. a) Galvanostatic charge-discharge test of the LCNO and LCO electrodes at 25°C, where the operating voltage range of 3.0–4.45 V (vs.  $\text{Li}/\text{Li}^+$ ) with charge and discharge of 1C. b) Voltage profiles corresponding to 1<sup>st</sup>, 5<sup>th</sup>, 25<sup>th</sup>, 50<sup>th</sup>, and 100<sup>th</sup> cycles. (c) Rate performance from 0.2 C to 5 C measured at 25 °C. d) Cycling performance of LCNO/Gr and LCO/Gr full-cells for 500 cycles.

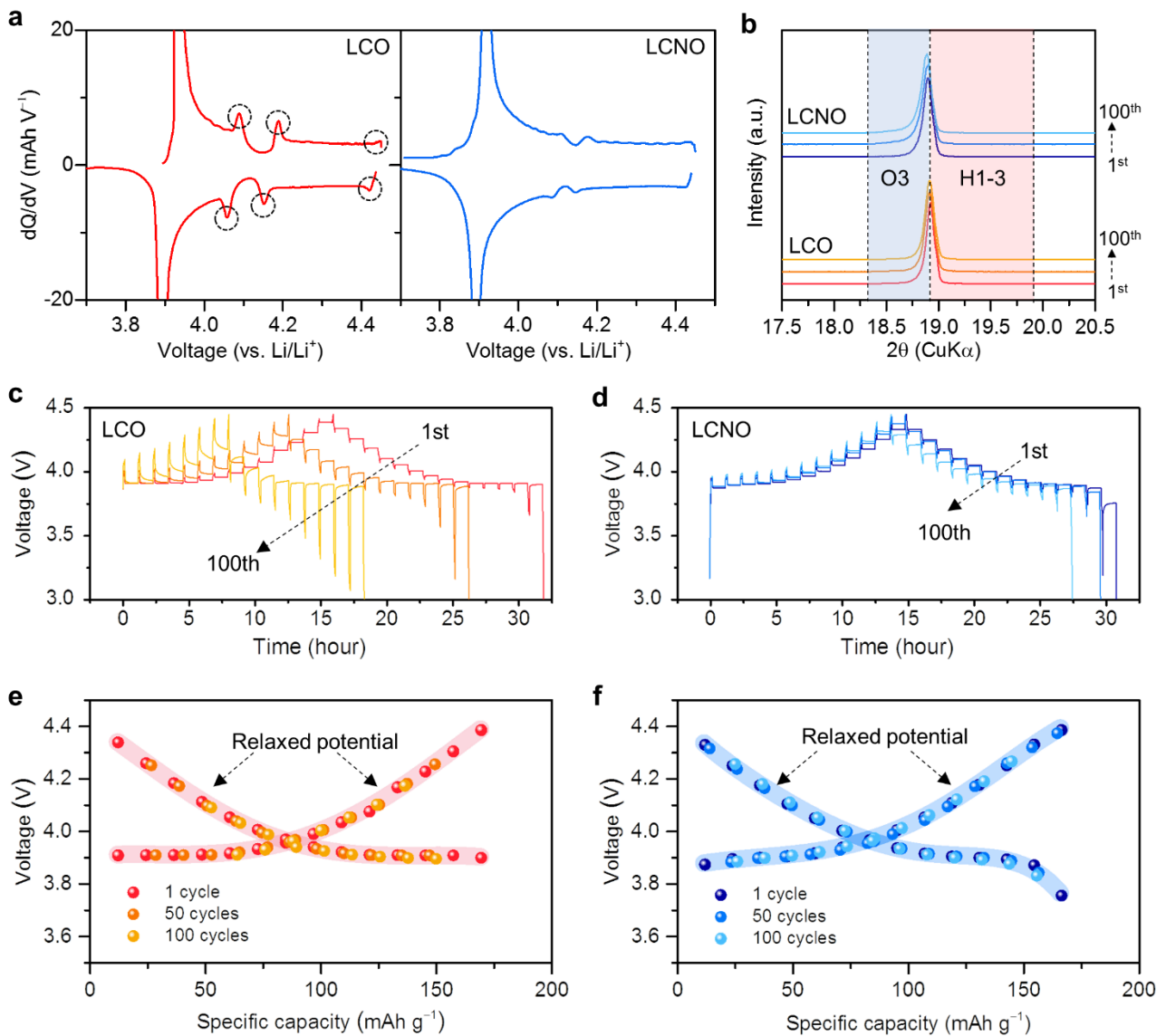


**Figure 2.** Electrochemical analyses of LCO and LCNO electrodes. a) Comparison of  $dQ/dV$  plot for cell with LCO and LCNO electrode in the voltage range of 3.0–4.45 V (vs.  $\text{Li/Li}^+$ ). b) Magnified ex situ XRD patterns between  $2\theta=17.5^\circ$  and  $20.5^\circ$  for 1<sup>st</sup>, 50<sup>th</sup> and 100<sup>th</sup> cycled LCO and LCNO. c-d) Voltage-time profiles of GITT for LCNO and LCO measured at 1<sup>st</sup>, 50<sup>th</sup> and 100<sup>th</sup> cycle, and (e-f) their voltage profiles under OCV conditions.

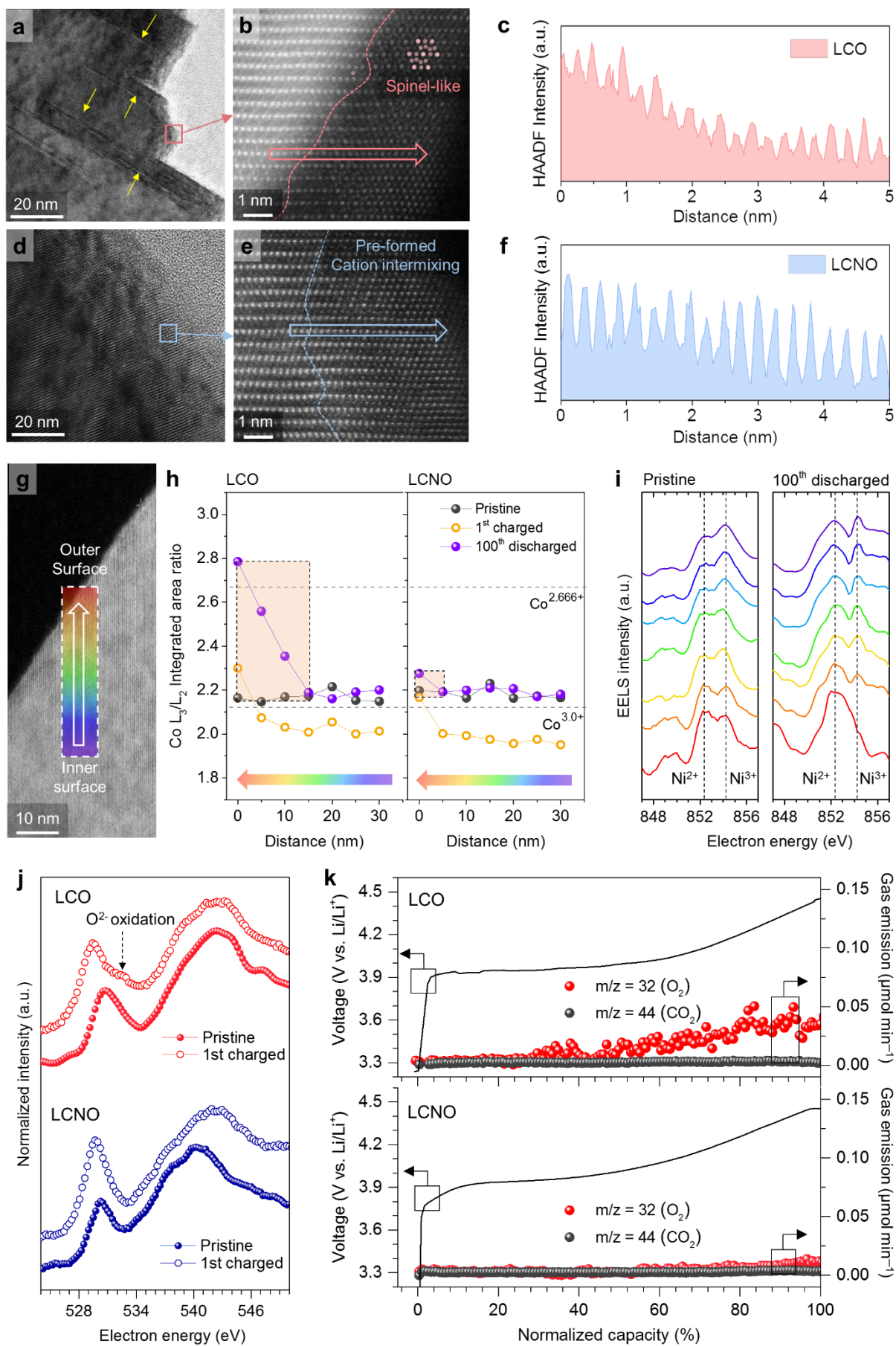


**Figure 3.** Stabilized LCNO surface showing less reconstruction, TM reduction and oxygen loss. a)

Surface microstructure of the LCO with micro-cracks after 100 cycles at 25°C half-cell, b) Magnified HAADF-STEM images corresponding to selected region of (a), showing Co<sub>3</sub>O<sub>4</sub>-like spinel. c) Declining HAADF-signal profile of the cycled LCO for selected region in (b). d) Surface microstructure of 100<sup>th</sup> cycled LCNO showing no cracks, e) Magnified HAADF-STEM image corresponding selected region of (d), showing inner and outer surface were stably maintained as layered and cation-mixing structure, respectively. f) Well-maintained HAADF-signal profile of the cycled LCNO for selected region in (e). g) Schematic EELS scanning pathway (0 to 35 nm from surface). h) Co L<sub>3</sub>/L<sub>2</sub> ratio analysis based on the collected Co L-edge at each state. The black dotted-lines indicate the oxidation state of Co as 2.66<sup>+</sup> and 3.00<sup>+</sup> (from top to bottom), respectively. Co L<sub>3</sub>/L<sub>2</sub> ratio for pristine, 1<sup>st</sup> charged and 100<sup>th</sup> discharged LCO and LCNO, showing less Co reduction for LCNO. (i) Ni L<sub>3</sub>-edge spectra for the pristine and cycled LCNO showing more Ni reduction at the surface and after cycling. j) The comparison between pre-edge of O K-edge EELS spectra corresponding to the outermost surface region for each pristine and 1<sup>st</sup> charged LCO and LCNO, suggesting less oxidization of O<sup>2-</sup> in LCNO surface. k) *In situ* DEMS analyses in coin-type half cell with LCO and LCNO during first charge.

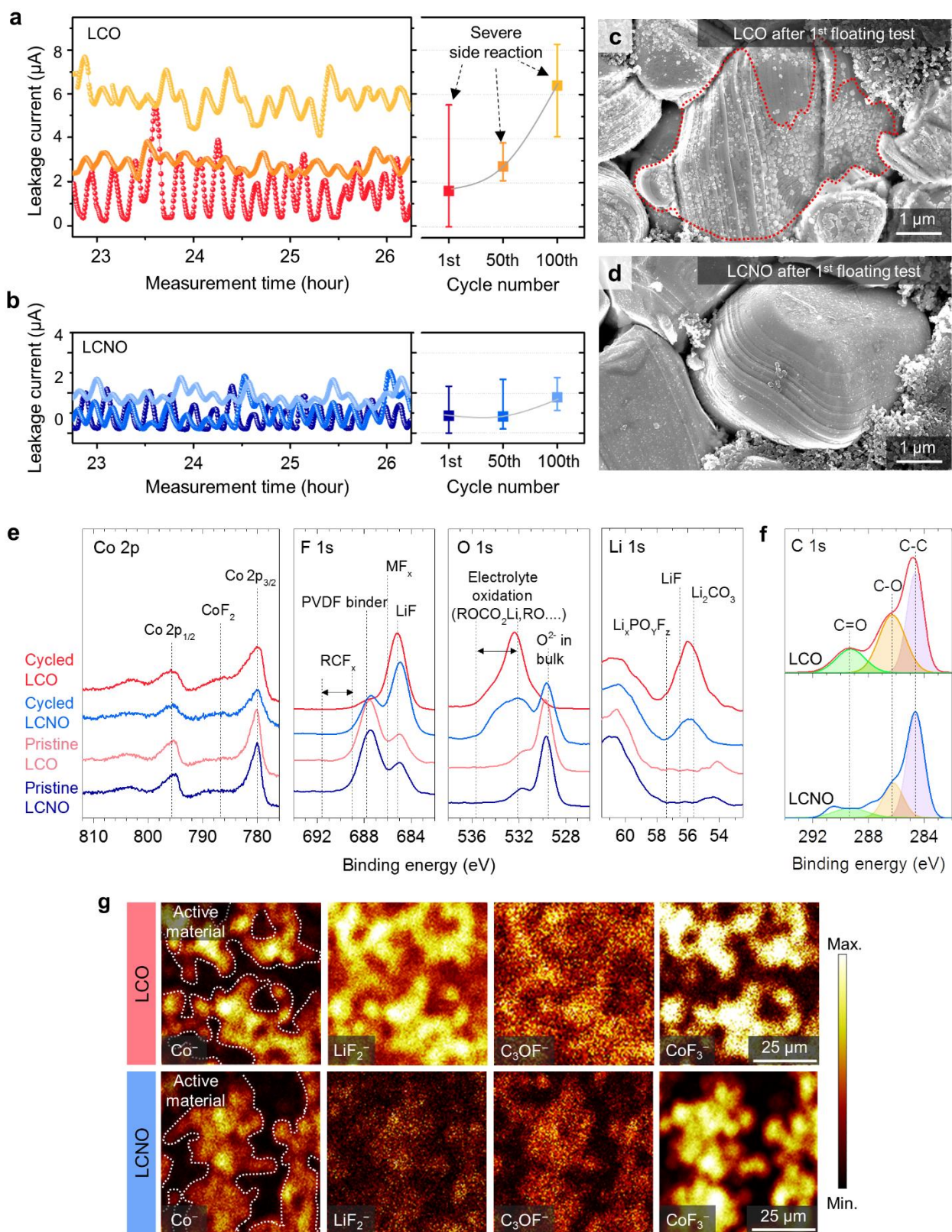


**Figure 4.** Investigating surface reactivity of cathode to electrolyte and suppressed CEI formation at surface. Leakage current of 1<sup>st</sup>, 50<sup>th</sup> and 100<sup>th</sup> cycled a) LCO and b) LCNO in floating tests. SEM of c) LCO and d) LCNO after floating tests for electrodes after 1<sup>st</sup> cycle. e) XPS spectroscopic data of LCO and LCNO electrodes before/after cycling: Co 2p, F 1s, O1s and Li 1s. Spectra of the cycled

and pristine electrode are displayed from the top to bottom. f) XPS spectroscopic data after cycling: C 1s. Note that the C 1s peaks characteristics of C–O (C 1s, 286eV) and C=O (C 1s, 289 eV) bond in approximately 2:1 ratio, an indicator of PEC evolution, are significantly observed in cycled LCO. g) Top view TOF-SIMS data for LCO and LCNO after cycling. The active material in cycled LCNO electrodes are less covered by CEI, mainly composed of organofluorines compound ( $C_3OF^-$ ) and HF attack resultant species ( ${}^7LiF_2^-$ ,  $CoF_3^-$ ).

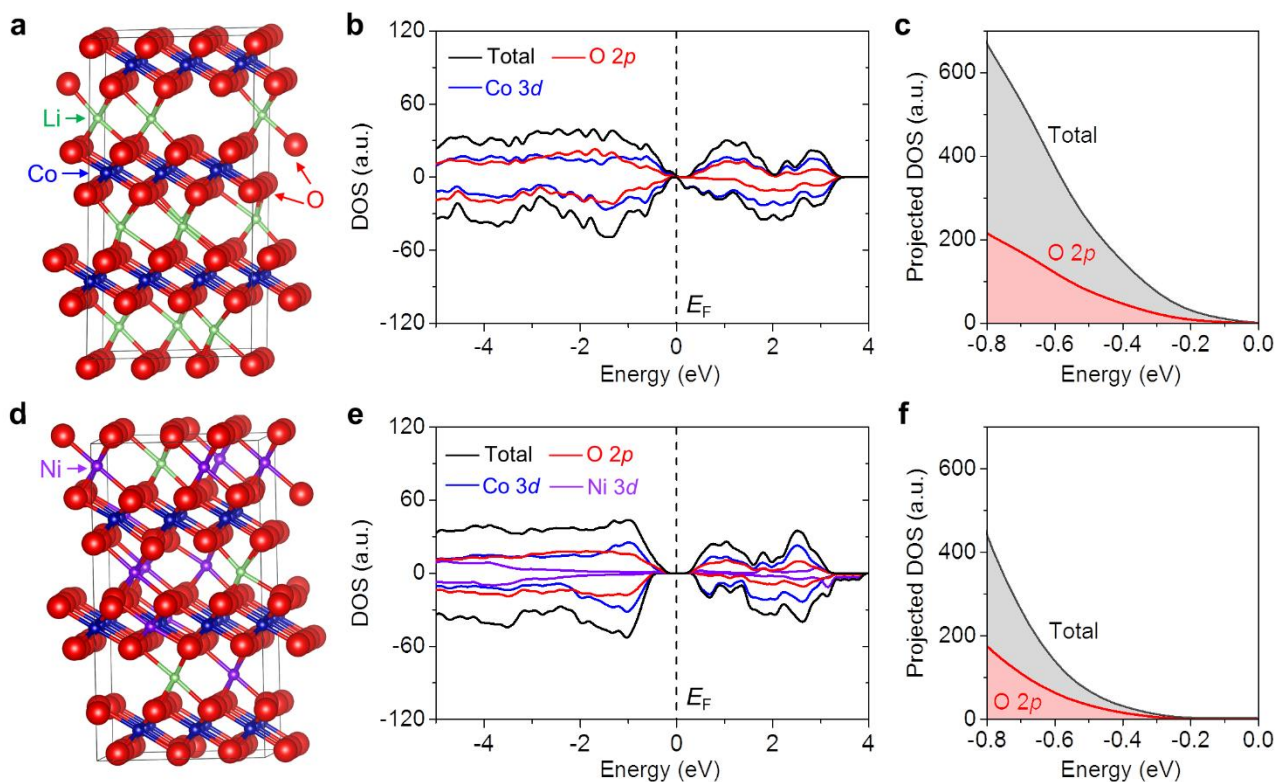


**Figure 5.** First-principles calculations showing less DOS around Fermi level for LCNO. (a) Atomic structure, (b) DOS and (c) available states at  $-0.8-0$  eV below Fermi level of  $\text{Li}_{0.333}\text{CoO}_2$  simulating delithiated LCO. (d) Atomic structure, (e) DOS and (f) available states at  $-0.8-0$  eV below Fermi level of  $\text{Li}_{0.111}\text{Ni}_{0.296}\text{Co}_{0.926}\text{O}_2$  simulating delithiated cation-mixed surface phase of LCNO. Fermi level is set to be 0 eV.

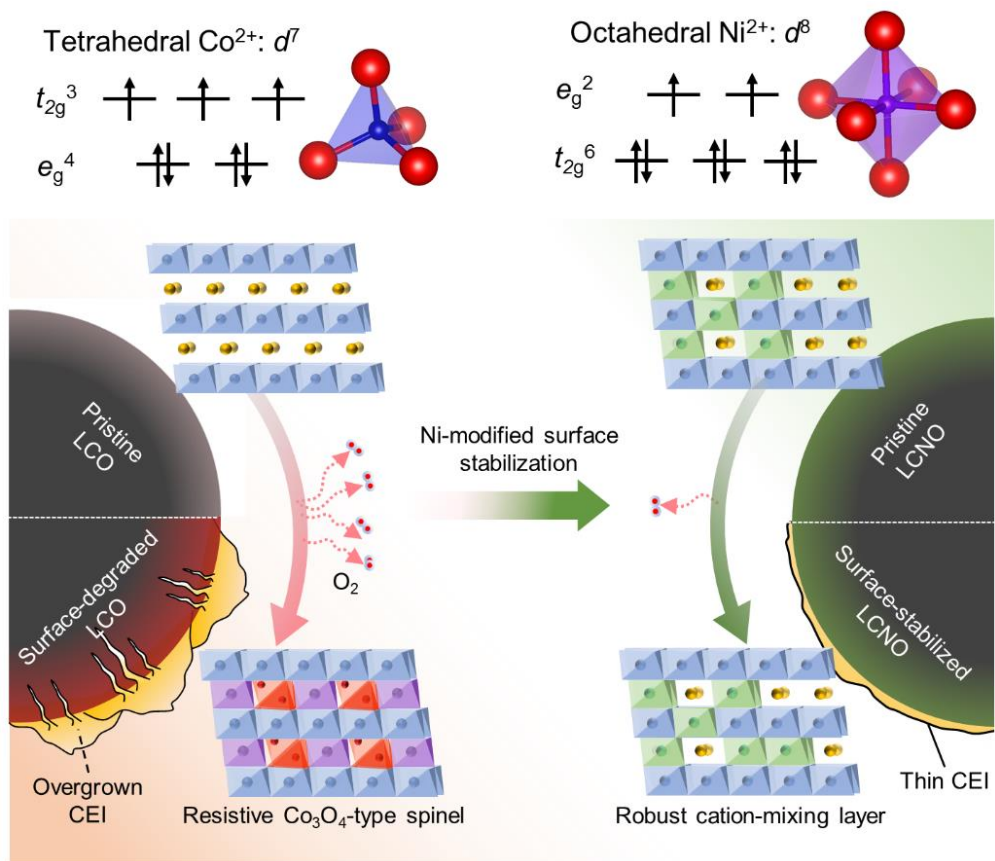


**Figure 6.** Schematic degradation mechanism of LCO and LCNO.